



Comparison of Design Tools for Stress Analysis of Adhesively Bonded Joints

Scott E. Stapleton
University of Massachusetts Lowell, Lowell, Massachusetts

Bertram Stier and Stephen Jones
Collier Research Corporation, Newport News, Virginia

Andrew C. Bergan and David W. Sleight
Langley Research Center, Hampton, Virginia

Brett A. Bednarczyk
Glenn Research Center, Cleveland, Ohio

Alana Zahn
Langley Research Center, Hampton, Virginia

Babak Farrokh and Kenneth N. Segal
Goddard Space Flight Center, Greenbelt, Maryland

NASA STI Program . . . in Profile

Since its founding, NASA has been dedicated to the advancement of aeronautics and space science. The NASA Scientific and Technical Information (STI) Program plays a key part in helping NASA maintain this important role.

The NASA STI Program operates under the auspices of the Agency Chief Information Officer. It collects, organizes, provides for archiving, and disseminates NASA's STI. The NASA STI Program provides access to the NASA Technical Report Server—Registered (NTRS Reg) and NASA Technical Report Server—Public (NTRS) thus providing one of the largest collections of aeronautical and space science STI in the world. Results are published in both non-NASA channels and by NASA in the NASA STI Report Series, which includes the following report types:

- **TECHNICAL PUBLICATION.** Reports of completed research or a major significant phase of research that present the results of NASA programs and include extensive data or theoretical analysis. Includes compilations of significant scientific and technical data and information deemed to be of continuing reference value. NASA counter-part of peer-reviewed formal professional papers, but has less stringent limitations on manuscript length and extent of graphic presentations.
- **TECHNICAL MEMORANDUM.** Scientific and technical findings that are preliminary or of specialized interest, e.g., “quick-release” reports, working papers, and bibliographies that contain minimal annotation. Does not contain extensive analysis.
- **CONTRACTOR REPORT.** Scientific and technical findings by NASA-sponsored contractors and grantees.
- **CONFERENCE PUBLICATION.** Collected papers from scientific and technical conferences, symposia, seminars, or other meetings sponsored or co-sponsored by NASA.
- **SPECIAL PUBLICATION.** Scientific, technical, or historical information from NASA programs, projects, and missions, often concerned with subjects having substantial public interest.
- **TECHNICAL TRANSLATION.** English-language translations of foreign scientific and technical material pertinent to NASA's mission.

For more information about the NASA STI program, see the following:

- Access the NASA STI program home page at <http://www.sti.nasa.gov>
- E-mail your question to help@sti.nasa.gov
- Fax your question to the NASA STI Information Desk at 757-864-6500
- Telephone the NASA STI Information Desk at 757-864-9658
- Write to:
NASA STI Program
Mail Stop 148
NASA Langley Research Center
Hampton, VA 23681-2199



Comparison of Design Tools for Stress Analysis of Adhesively Bonded Joints

Scott E. Stapleton

University of Massachusetts Lowell, Lowell, Massachusetts

Bertram Stier and Stephen Jones

Collier Research Corporation, Newport News, Virginia

Andrew C. Bergan and David W. Sleight

Langley Research Center, Hampton, Virginia

Brett A. Bednarczyk

Glenn Research Center, Cleveland, Ohio

Alana Zahn

Langley Research Center, Hampton, Virginia

Babak Farrokh and Kenneth N. Segal

Goddard Space Flight Center, Greenbelt, Maryland

National Aeronautics and
Space Administration

Glenn Research Center
Cleveland, Ohio 44135

Acknowledgments

The NASA authors acknowledge the support from the Space Technology Mission Directorate Composite Technologies for Exploration Project and the Aeronautics Research Directorate Transformational Tools and Technologies Project.

Trade names and trademarks are used in this report for identification only. Their usage does not constitute an official endorsement, either expressed or implied, by the National Aeronautics and Space Administration.

Level of Review: This material has been technically reviewed by technical management.

Available from

NASA STI Program
Mail Stop 148
NASA Langley Research Center
Hampton, VA 23681-2199

National Technical Information Service
5285 Port Royal Road
Springfield, VA 22161
703-605-6000

This report is available in electronic form at <http://www.sti.nasa.gov/> and <http://ntrs.nasa.gov/>

Comparison of Design Tools for Stress Analysis of Adhesively Bonded Joints

Scott E. Stapleton
University of Massachusetts Lowell
Lowell, Massachusetts 01854

Bertram Stier and Stephen Jones
Collier Research Corporation
Newport News, Virginia 23606

Andrew C. Bergan and David W. Sleight
National Aeronautics and Space Administration
Langley Research Center
Hampton, Virginia 23666

Brett A. Bednarczyk
National Aeronautics and Space Administration
Glenn Research Center
Cleveland, Ohio 44135

Alana Zahn
National Aeronautics and Space Administration
Langley Research Center
Hampton, Virginia 23666

Babak Farrokh and Kenneth N. Segal
National Aeronautics and Space Administration
Goddard Space Flight Center
Greenbelt, Maryland 20771

Abstract

Despite the proliferation and flexibility of high fidelity finite element models, lower fidelity models remain commonly used in adhesively bonded joint design. These design models can save both computational and user time due to their simplicity and ease of use. The current study involves a detailed assessment of the local stress fields predicted by four bonded joint design models: A4EI, HyperSizer, Joint Element Designer, and a Continuum Solid Shell Finite Element model. All models were compared with a high fidelity, dense mesh finite element model as a benchmark. Six different double lap joint cases were compared with different combinations of features including metallic and composite adherends, a sandwich core, and doubler tapers. As expected, the order of the model's through-thickness displacement interpolation was a significant driver of accuracy. However, not every case requires higher order interpolation to achieve accurate results.

1.0 Introduction

With the increasing demand for fiber reinforced composites in lightweight structures, adhesively bonded joints are becoming more prevalent than ever. Bolts and rivets require holes, which result in severed fibers, cause significant stress concentrations, and can cause premature failure in composite materials. Adhesives spread the load more evenly over the composite while facilitating a lighter overall structure. Reductions in part count and touch labor can also result in significant cost reductions for adhesively bonded joints. The structural adhesive market in Europe has been forecasted to reach 67,000 tons by 2015, a growth of over 13 percent since 2008 (Ref. 1).

Analytical models for stress analysis have long been a part of initial adhesive joint design, analysis, and sizing. Despite the rise of general finite element software and methods, analytical design models remain a preferred method for fast and simple joint analysis due to stress singularities that are typical in bonded joints near reentrant corners. While these analytical methods can yield accurate results, the models are constructed on the foundation of kinematic, geometrical, and material simplifications, along with assumptions that allow closed form or semi-closed form solutions. This study compares and contrasts three analytical methods and a relatively efficient finite element model that are under assessment by NASA for use in launch vehicle design. The analytical methods are: (1) The A4EI code based on the methods of Hart-Smith (Refs. 2 and 3), (2) The HyperSizer joints analysis capability based on extensions of the methods of Mortensen and Thomsen (Ref. 4), and (3) the joint element designer (JED) based on the methods of Stapleton and co-workers (Ref. 5). The results from these methods are compared with high-fidelity 3-D finite element results to show the implications of the assumptions used in each method for several exemplar bonded joint configurations. The joint configurations considered are: (1) double lap joint with aluminum adherends, (2) double lap joint with composite adherends, (3) stepped double lap joint with composite adherends, (4) double lap joint with composite adherends containing a honeycomb core, and (5) stepped double lap joint with composite adherends containing a honeycomb core.

2.0 Joint Configuration

Different joint configurations were analyzed in order to compare the joint analysis tools. The analyzed joint configurations, discussed in Section 2.0, range from simple to increasingly complex to pinpoint differences in the results from the various methods compared with the benchmark high-fidelity finite element results. In this section, the material properties, geometries, and boundary conditions employed for the bonded joint cases are presented.

2.1 Materials

Material properties for the composite system and adhesive were obtained from open literature when possible. If data was not readily available for certain properties, notional values were assumed. Because this study sought to compare the behavior of several tools for identical problems rather than determine their absolute accuracy, notional values are acceptable. Table 1 to Table 5 provide the material properties for the aluminum, carbon/epoxy composite, aluminum honeycomb, and film adhesive materials used in this study. All properties are the average of tension and compression unless otherwise noted.

TABLE 1.—ALUMINUM PROPERTIES
(ALL NOTIONAL)

Property	Value	Units
E_{11}	10.0	Msi
E_{22}	10.0	Msi
E_{33}	10.0	Msi
G_{12}	3.85	Msi
ν_{12}	0.300	----
G_{13}	3.85	Msi
G_{23}	3.85	Msi
ν_{23}	0.300	----
ν_{13}	0.300	----

TABLE 2.—AVERAGE IM7/8552-1 PLY
PROPERTIES (REF. 6)

Property	Value	Units
E_{11}	21.3	Msi
E_{22}	1.26	Msi
E_{33}	1.26	Msi
G_{12}	0.749	Msi
ν_{12}	0.320	----
G_{13}	0.749	Msi
G_{23}	0.435	Msi
ν_{23}	0.450	----
ν_{13}	0.320	----
t_{ply}	0.0072	in.

TABLE 3.—AVERAGE T650 / 5320-1 PLAIN
WEAVE PLY PROPERTIES (REF. 7)

Property	Value	Units
E_{11}	9.28	Msi
E_{22}	9.28	Msi
E_{33}	^a 1.26	Msi
G_{12}	0.735	Msi
ν_{12}	0.053	----
G_{13}	^b 0.592	Msi
G_{23}	^b 0.592	Msi
ν_{23}	^c 0.106	-----
ν_{13}	^c 0.106	-----
t_{ply}	0.0077	in.

^aAssumed to be equal to E_{33} for the IM7/8552-1 system.

^bAssumed equal to the average of IM7/8552-1 G_{12} and G_{23} .

^cAssumed to be equal to $2\nu_{12}$.

TABLE 4.—PLASCORE 3/16 in. 3.1 PCF
HONEYCOMB CORE (PAMG-XR1 5056)
PROPERTIES (REF. 8)

Property	Value	Units
E_{11}	^a 100	psi
E_{22}	^a 100	psi
E_{33}	97000	psi
G_{12}	^a 100	psi
ν_{12}	^b 0.5	----
G_{13}	45000	psi
G_{23}	20000	psi
ν_{23}	^a 0.001	-----
ν_{13}	^a 0.001	-----
t_{core}	1	in.

^aNotional, assumed to be low.

^bAssumed incompressibility in this plane.

TABLE 5.—FILM ADHESIVE PROPERTIES
(ALL NOTIONAL)

Property	Value	Units
E_{11}	234000	psi
E_{22}	234000	psi
E_{33}	234000	psi
G_{12}	87800	psi
ν_{12}	0.330	----
G_{13}	87800	psi
G_{23}	87800	psi
ν_{23}	0.330	----
ν_{13}	0.330	----
$t_{adhesive}$	0.005	in.

2.2 Geometries and Boundary Conditions

As stated previously, the cases were conceived to progressively include increasing amounts of complexity to compare different features of the models. The final geometry (Cases 5 and 6) resembles a joint of interest for NASA, and the other examples were created by dropping one feature. The geometries are shown in Figure 1 and the corresponding boundary conditions are shown in Figure 2. Due to symmetry of the geometry and loading, only one half of each joint was modeled with symmetry boundary conditions in the middle.

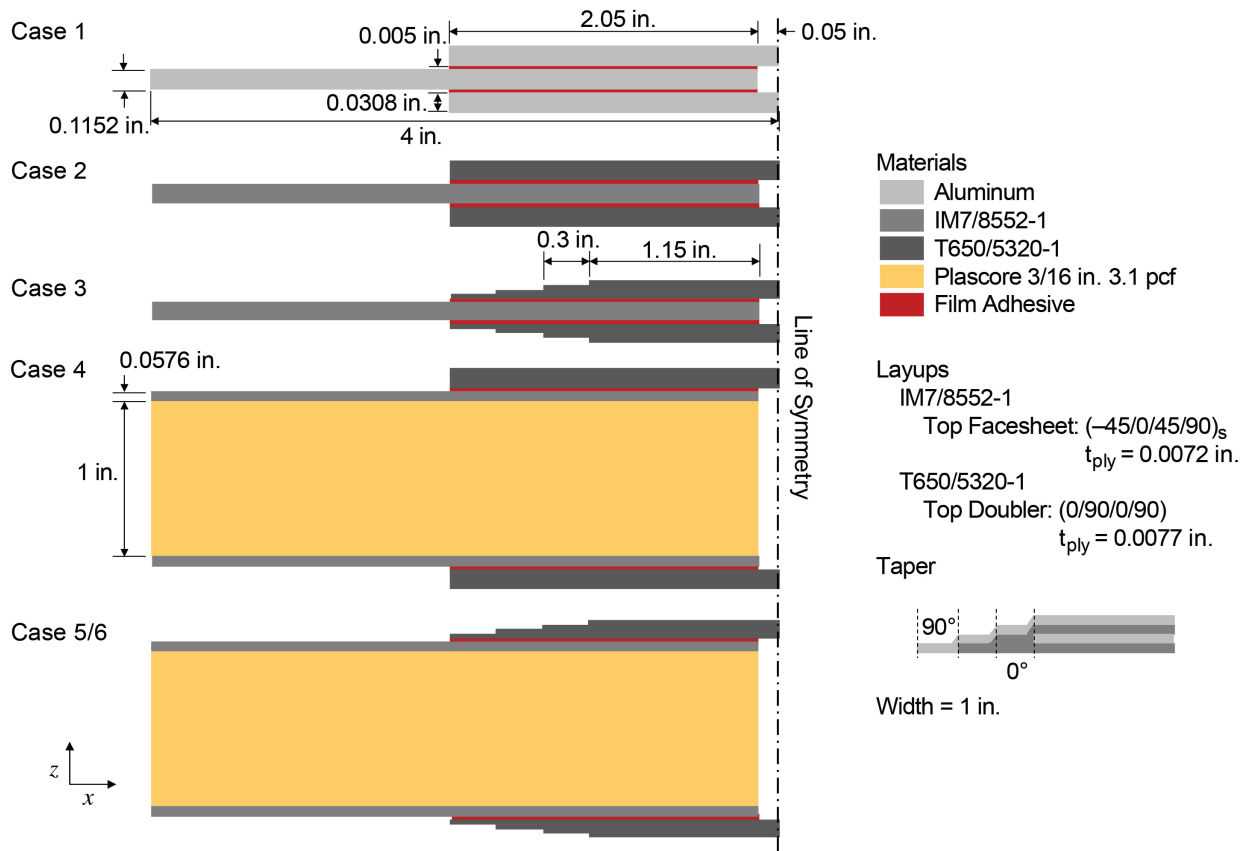


Figure 1.—Geometry, materials, and layup of the six cases used to compare the analysis tools.

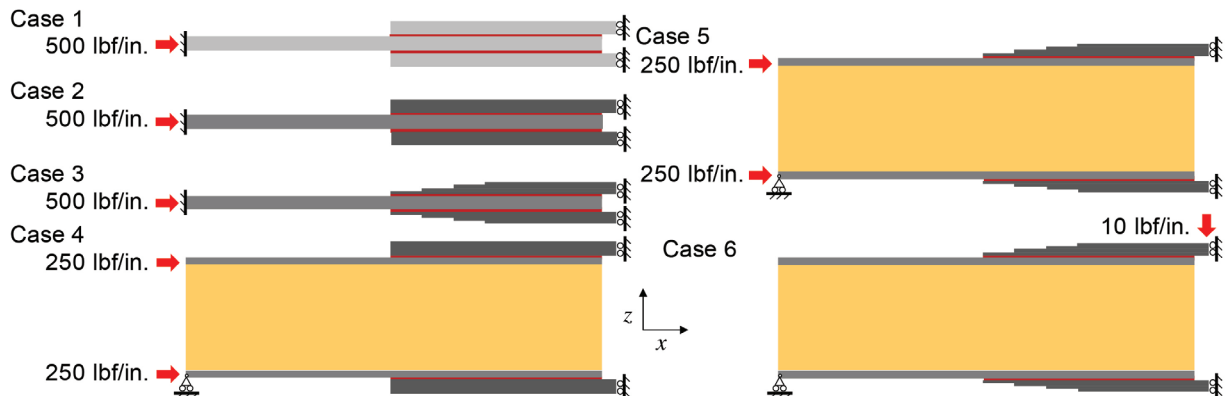


Figure 2.—Boundary conditions for six cases used to compare the design models.

Case 1 is a double lap joint with aluminum adherends under compression with the adherend restricted from rotation and vertical displacement at the point of loading. Case 2 has layered composite materials as the adherends, with the layups and materials noted in the Figure 1. The adherend was made by putting the two facesheets from the sandwich cases (Cases 3 to 6) together in one layup. Case 3 is a replica of Case 2 except that the doublers are stepped, dropping one ply per step. Case 4 is like Case 2 except with a core. The load was split between two facesheets, and only the lower facesheet is restricted from vertical displacement at the point of loading. Finally, Cases 5 and 6 are the same geometry as Case 4 except with stepped doublers, and Case 6 is in a 3-pt bending configuration rather than axial compression.

Looking at the cases, Case 1 is the simplest, Case 2 adds composite adherends, Case 3 adds a taper, Case 4 adds a core with no taper, Case 5 adds a taper and core, and 6 adds load case complexity. In this way, differences in models can be isolated to specific features of the joints, one feature at a time.

2.3 Simplifying Assumptions

Although a total of six cases are studied in this work, several design features typical of double lap/double strap joints used in practice are not considered. First, the gap between the adherends (right side in Figure 1) is treated as a void herein whereas it is common to use a polymer filler material for manufacturability, which may affect the local stress distribution and the failure process. A second simplification is that the adhesive layer is treated with a linear elastic constitutive behavior when it is known that plastic deformation and fracture may occur. To be consistent with assuming a linear behavior in the adhesive, the applied loads are relatively low such that no significant plastic deformation or other nonlinearities are expected. It should be noted that all methods considered herein are capable of including nonlinear adhesive behavior. Another simplifying assumption is that an explicit adhesive layer is included in all cases; in some instances a co-cured design is used where the doubler resin adheres the doubler to the adherend and no separate adhesive layer is used. A fourth simplifying assumption is that the doubler drop-off sequence is held at a constant taper angle with the same ply drop sequence for all cases such that the stresses due the ply drops are relatively low. In some designs, the doubler ply drop region may introduce much higher stress and therefore be more critical (Ref. 9). Lastly, it should be recognized that in practical structures, joints experience combined load conditions. Therefore, this paper represents a study of only elastic stress fields predicted by several rapid analysis tools in response to relatively simple loading conditions. It is of great interest to extend and apply rapid joint analysis tools to address several of the practical joint design features that have been omitted from this study.

3.0 Models

3.1 A4EI

A4EI is software developed based on the methods of Hart-Smith (Refs. 2 and 10), which consider a 1-D semi-closed form solution for bonded joints. The adherends, which may be stepped, are modeled as truss members (with no bending) with homogenized section stiffnesses as input. The adhesive is treated as a bed of shear springs that can have an elastic-perfectly plastic shear response. The formulation involves application of equilibrium conditions to arrive at closed-form expressions for the axial deformation along the adherends. Integration constants appearing in these expressions, however, are determined via an iterative approach that can have convergence difficulties (Ref. 2). The A4EI solution provides the adhesive shear stresses and strains, as well as an average axial stress in the adherends, along the bonded joint. Given corresponding strength values as input, the strength of the joint can be determined. Notably, many versions of the code (including that used herein) do not include the adhesive

peel stress in the formulation, and no ply-level stresses are calculated in the case of composite adherends, although Hart-Smith does provide a simple solution for the approximate peak peel stress at the end of the joint (Ref. 3). This limits A4EI's ability to predict delamination in the adherends, which is a common failure mode in composite bonded joints. Nevertheless, while the software dates from the 1970's, it is still used and can provide a reasonable estimate of adhesive shear stresses that can be used to size a joint given adhesive allowables.

3.2 HyperSizer

The bonded composite joint analysis capability within the HyperSizer structural sizing software (Ref. 11) is based on Mortensen and Thompsen's (Ref. 4) unified approach with extensions to compute ply level in-plane and interlaminar stresses, apply pressure loading, determine margins of safety based on a wide array of bonded joint specific failure criteria, and evaluate bond-line cracks with the Virtual Crack Closure Technique, (see Refs. 12 to 14) for details. The joint adherends are treated as plates in generalized cylindrical bending, which allows for application uniform strain and uniform curvature in the direction normal to the joint analysis plane (i.e., the y -direction in Figure 1). The adherends are arbitrary composite laminates governed by classical lamination theory. The adhesive is treated as a continuously distributed layer of normal and shear springs whose constitutive response may be nonlinear. Boundary conditions are applied in the form of displacements/rotations or force/moment resultants.

The joint is divided into regions whose governing linear first-order differential equations are developed based on direct application of equilibrium. These equations are solved via the multisegment method of integration presented by Mortensen and Thompsen (Ref. 4). The joint regions are each divided into small segments, and the solution of each segment is determined using direct integration. Continuity between these segments and between the joint regions is enforced, while accounting for any midplane shifts because of changes in thickness. This solution procedure provides the adherend level results (mid-plane displacements, strains, and curvatures and force and moment resultants) along the joint x -direction (Figure 1). The ply level in plane stresses are then determined via Classical Lamination Theory, and the interlaminar stresses are calculated via integration of the equilibrium equations (see Ref. 15 for details).

Cases 1 to 3, considered herein, represent standard nonstepped and stepped double lap joints that were considered by Mortensen and Thompsen (Ref. 9) and that have been included within the HyperSizer bonded joints capability for some time. Cases 4 and 5, in which one adherend is honeycomb sandwich panel, could be analyzed using the standard double lap joint capability provided the core material is simply treated as a ply and the honeycomb sandwich panel treated as a laminate. However, it is also possible to treat the core material as an additional layer of normal and shear springs, similar to how the adhesives are treated in the formulation. This better captures the physics of the core behavior as it enables the core material to deform in the through-thickness direction. As such, a new sandwich double lap joint concept that treats the core as an additional adhesive layer was formulated and implemented within the HyperSizer joints capability.

The HyperSizer geometry for the Cases 5 and 6 joint is shown in Figure 3 and Figure 4. The grids shown in the geometry details actually represent analysis points in the model adherends (as opposed to elements typically shown for finite element models). In the x -direction, Regions 1 and 3 were divided into 25 segments, each with 5 points. In Region 2, each of the four steps were divided into 5 segments, each with 5 points. In the z -direction, 15 analysis points were used per ply. Again, these z -direction analysis points were used to determine the interlaminar stresses through numerical integration. The adhesives and core do not participate in this integration as they are modeled as distributed layers of normal and shear springs. Thus, three output points were used for the adhesive and core: one at the top and bottom and one in the middle.

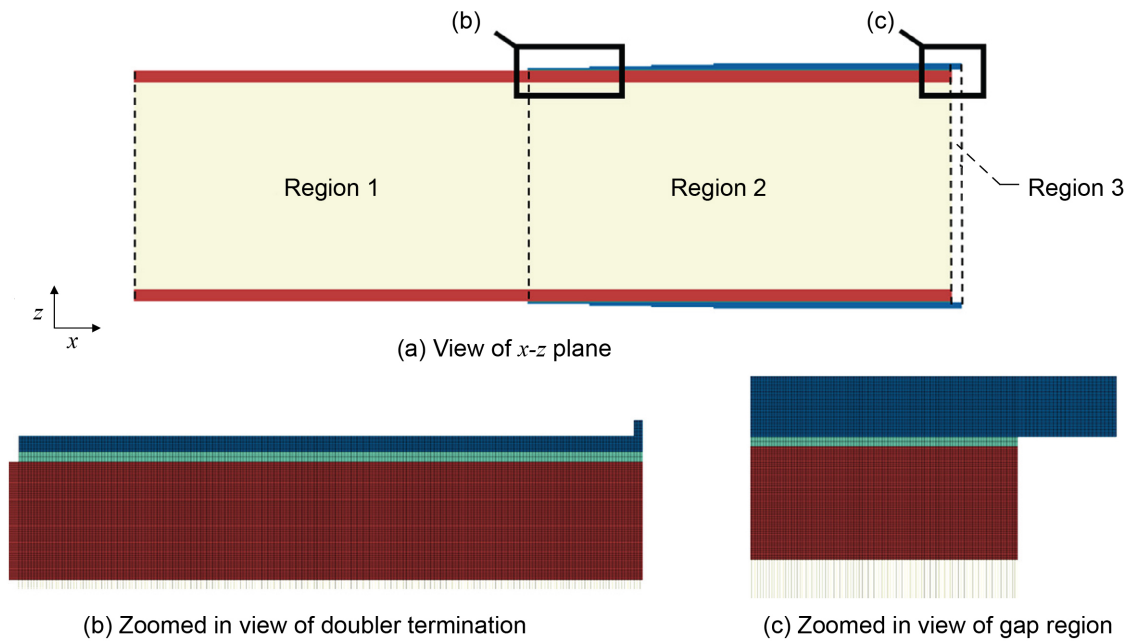


Figure 3.—HyperSizer bonded joint analysis geometry for Case 5.

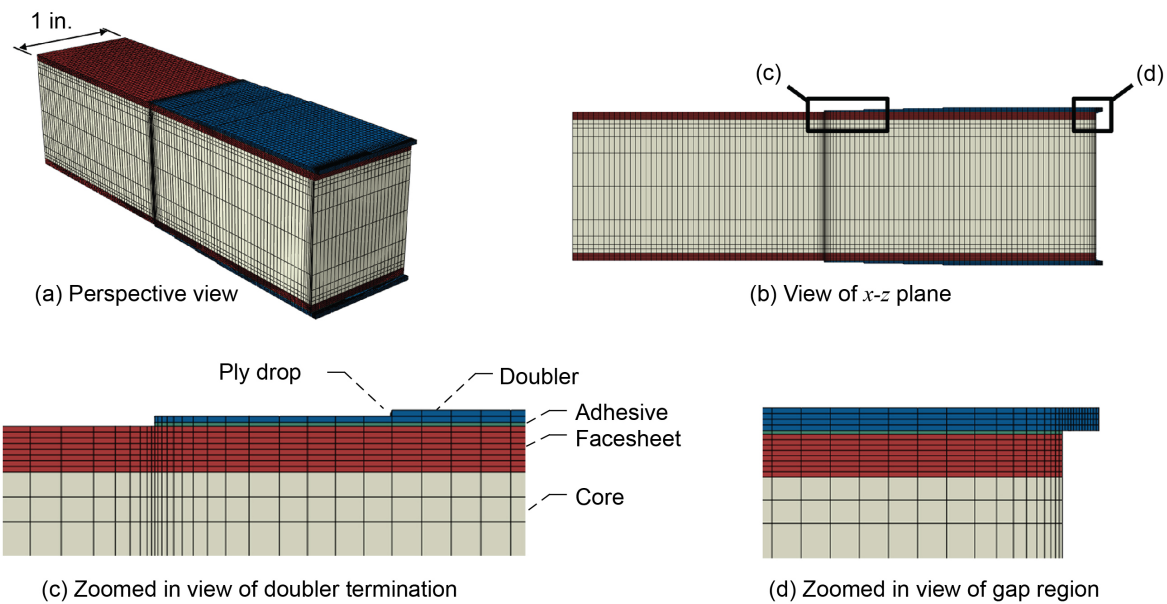


Figure 4.—Parametric continuum solid shell FEM.

3.3 Joint Element Designer (JED)

The Joint Element Designer (JED) software was originally created to integrate finite element software and semi-analytical joint models (Refs. 5 and 16). The model uses the same assumptions for the adherends as the HyperSizer method: beams under cylindrical bending, although the beams can be Euler-Bernoulli or Timoshenko with shear deformations. Multiple models have been implemented for the core/adhesive layers, with distinctions having to do with the interpolation of displacements through the thickness or the constitutive model. Linear interpolation through the thickness is generally used for adhesives due to their thin nature, while sandwich cores typically require higher order quadratic functions (Ref. 17). Though not utilized here, options such as nonlinear geometry (through co-rotational formulation),

crack growth, adaptive shape functions, and graded adhesives are available (Refs. 18 to 20). The model utilizes a standard finite element solution procedure for beam elements, with a few key differences. Rather than polynomial functions chosen for shape functions along the axial axis, the structural model is solved using the matrix exponential (Ref. 21). This results in shape functions that are determined rather than prescribed. This means that a single element is sufficient for a joint with linearly elastic materials as the shape functions are customized to the joint problem being considered. However, even in the elastic case, more elements may be needed along the length so improve solution stability. Finally, complex joints can be made by joining different elements at nodes like standard finite element software.

Since the HyperSizer method uses a linear variation of displacements through the core/adhesive thickness, to draw more of a distinction, the JED model in this study used the quadratic variation of displacements through the adhesive/core. The displacements in the core (or adhesive), $w_c(x, z)$ and $u_c(x, z)$, are assumed to be in the form of:

$$u_c(x, z) = a_0(x) + za_1(x) + z^2a_2(x) \quad (1)$$

and

$$w_c(x, z) = b_0(x) + zb_1(x) + z^2b_2(x) \quad (2)$$

where the functions $a_i(x)$ and $b_i(x)$ can be found in terms of the displacements at the interface between the adherend above and below the adhesive/core (assuming perfect bonding) and the displacement of the adhesive/core centerline. Thus, the energy can be formulated in terms of centerline displacements, which are only unknown in x , and the system of ODEs can be solved. Additionally, for this model, the stresses in the adhesive/core were assumed to be uncoupled, meaning that

$$D_c = \begin{bmatrix} E_{cxx} & 0 & 0 \\ 0 & E_{czz} & 0 \\ 0 & 0 & G_{cxz} \end{bmatrix} \quad (3)$$

where

$$\begin{aligned} \sigma_c &= D_c \epsilon_c, \\ \sigma_c &= [\sigma_{cxx} \quad \sigma_{czz} \quad \tau_{cxz}]^T \\ \text{and } \epsilon_c &= [\epsilon_{cxx} \quad \epsilon_{czz} \quad \gamma_{cxz}]^T \end{aligned} \quad (4)$$

Here, E_{cxx} , E_{czz} , and G_{cxz} are the elastic properties of the adhesive/core, whereas, σ_{cxx} , σ_{czz} , τ_{cxz} , ϵ_{cxx} , ϵ_{czz} , and γ_{cxz} are the stress and strain components of the adhesive/core.

While analyzing the sandwich joints (Cases 4 to 6), the combination of a thin adhesive layer and thick core in the same element caused instabilities due to vastly different magnitudes of eigenvalues in the coefficient matrix of the system of ODEs to be solved. Therefore, very small elements were needed in the x -direction in order to achieve a converged solution. Globally, a nominal element size of 0.01 in. was used, which translates to 226 elements total.

3.4 Parametric Continuum Solid Shell (CSS) FE

A parametric 3-D finite element model was developed using the python scripting interface for Abaqus for the joint cases with a sandwich adherend. The script was written and is being further developed at NASA Langley Research Center. By automating the finite element modeling process from pre to post-processing, the script enables relatively quick evaluation of joints with varying parameters.

The model is intended to be fast running for preliminary design evaluations. Therefore, the mesh refinement and element type were chosen to balance run time and stress field fidelity as follows. The mesh is shown in Figure 4 colored by component. The doubler, adhesive, and facesheet were each modeled with one layer of continuum solid shell elements (CSS8) per ply. The CSS element is formulated with seven incompatible modes to improve bending behavior and an assumed strain to mitigate locking (Refs. 22 and 23). The core was modeled with continuum solid elements with reduced integration (C3D8R) and enhanced hourglass control. The in-plane element edge length varied from 0.004 to 0.04 in. in the doubler region. In general, the mesh refinement used was found to be converged except immediately at the reentrant corners where stress singularities exist in linear analyses.

To facilitate comparison with the 2-D analysis methods, additional assumptions and approximations specific to this study were required. The dimension of the model along the joint axis (y -direction) was arbitrarily set to 1 in. and plane strain was assumed by enforcing zero y -direction displacement at all nodes. Linear analysis was conducted using Abaqus 2017. Typical runs times were on the order of 90 sec.

3.5 Benchmark: High Fidelity FEM

In order to establish a reference for the various comparisons, full 3-D continuum mechanics finite element analyses with high mesh density were carried out using the commercial finite element analysis (FEA) program Abaqus. The finite element meshes are shown in Figure 5. The objective for these models was to find “converged” stress fields – time or computational efficiency were low priority. The metallic adherends, as well as the adhesive layers, were discretely modeled as isotropic, homogeneous continua. Individual plies were discretely modeled as transversely isotropic and orthotropic continua for unidirectional and fabric composite layers, respectively. Each ply had individual material orientations assigned to capture the ply stacking and anisotropic effects. Ply drops were idealized as abrupt steps.

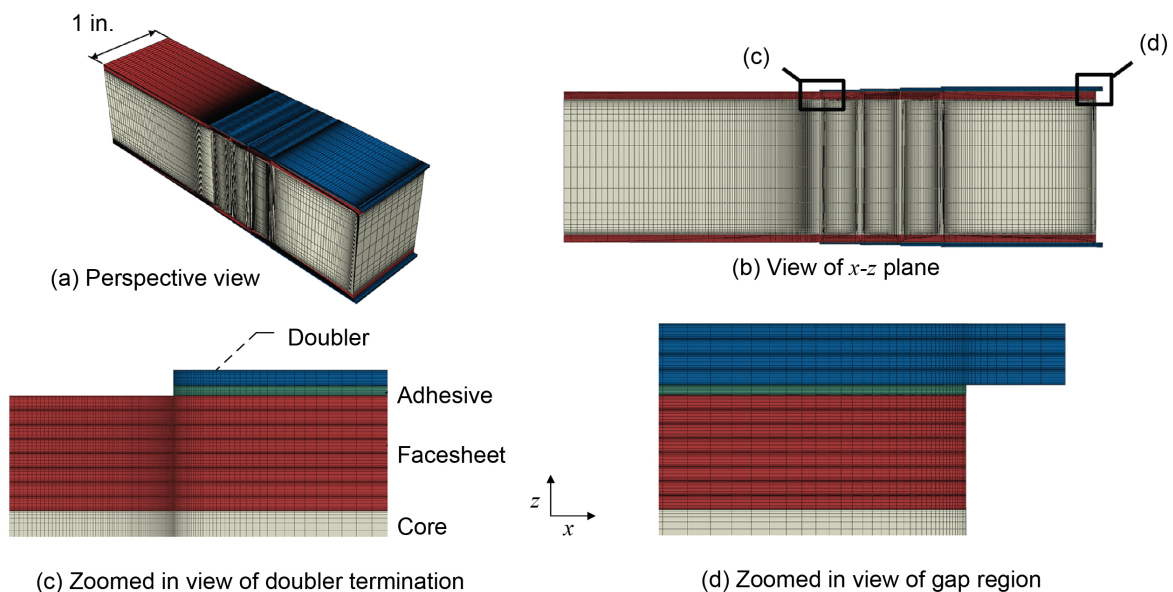


Figure 5.—High fidelity FEM used as a benchmark, showing details of the mesh at regions of highest refinement.

Biased mesh generation in both the longitudinal and thickness direction was utilized. In order to capture high stress gradients, the mesh density in the proximity to geometric discontinuities in longitudinal direction, such as ply drops, and in proximity to material discontinuities in thickness direction, such as interfaces between individual plies, core, or adhesive materials, was increased. At least ten 3-D linear continuum mechanics reduced integration elements (C3D8R) were used through the thickness of each ply, adhesive layer or metallic adherend. At least 20 elements were used through the thickness of the core. The convergence of the mesh density through the thickness was judged by observing the transverse shear and normal stress continuity through the thickness at the center of the width of the joint at a characteristic distance “inward” from both reentrant corners. The characteristic distance (facesheet half ply thickness) was chosen since it is a commonly used measure to step away from the stress singularity occurring at the edge of the reentrant corner. Similarly, the mesh density in the joint longitudinal direction was judged by the continuity of the peel and shear stress along the adhesive centerline at half width and thickness. The aspect ratios of the elements were kept reasonable to keep locking effects at a minimum.

Similar to the CSS finite element models, the width of the joint was arbitrarily chosen to be 1 in. All nodes were restrained in width direction to simulate plane strain conditions. Loads and boundary conditions were introduced using reference points and kinematic coupling constraints such that the conditions could effectively be applied to the neutral axis of the adherends in addition to effectively maintaining “plane remains plane” (plate) conditions at the boundary.

4.0 Results

Results are presented in two forms: line plots and contour plots. The line plots show the stress along the centerline of the top adhesive layer. The peel (σ_{zz}) and shear (τ_{xz}) stresses are considered critical for the adhesive and are each plotted for the six cases in Figure 6, Figure 8, Figure 10, Figure 12, Figure 14, and Figure 16. For the adherends, the axial stress (σ_{xx}) is the primary component. Additionally, delamination can be a major concern for composite adherends and the interlaminar stresses (σ_{zz} and τ_{xz}) have been considered. Contour plots of these stresses at critical regions for the six cases are presented in Figure 7, Figure 9, Figure 11, Figure 13, Figure 15, and Figure 18. The results for each of the six cases are presented here, followed by a discussion of the results in the next section. Note that CSS finite element models were only constructed for the cases with a core (Cases 4 to 6).

4.1 Case 1—Aluminum Adherends, No Steps, No Core

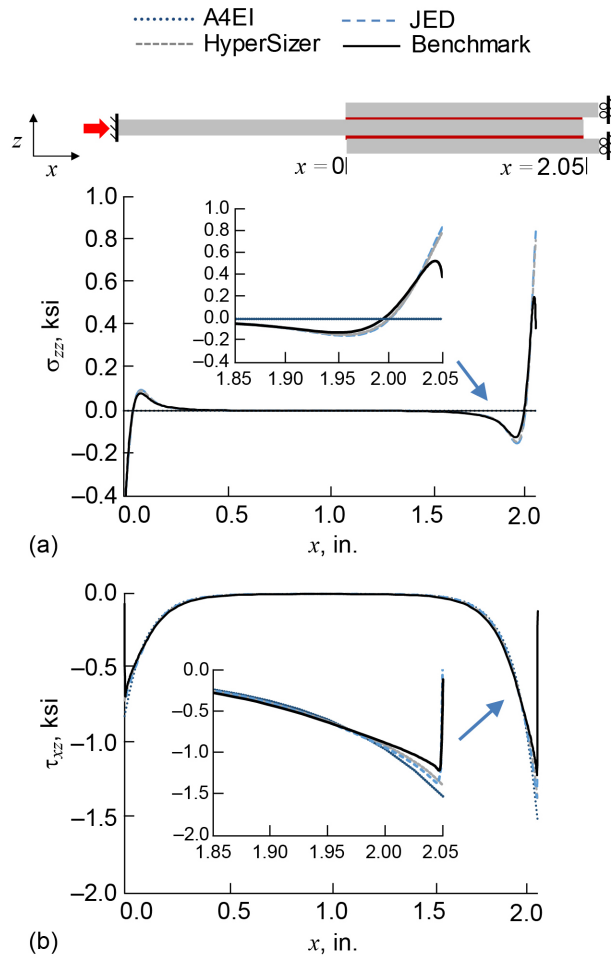


Figure 6.—Peel (a) and shear (b) stresses along the top adhesive centerline of Case 1.

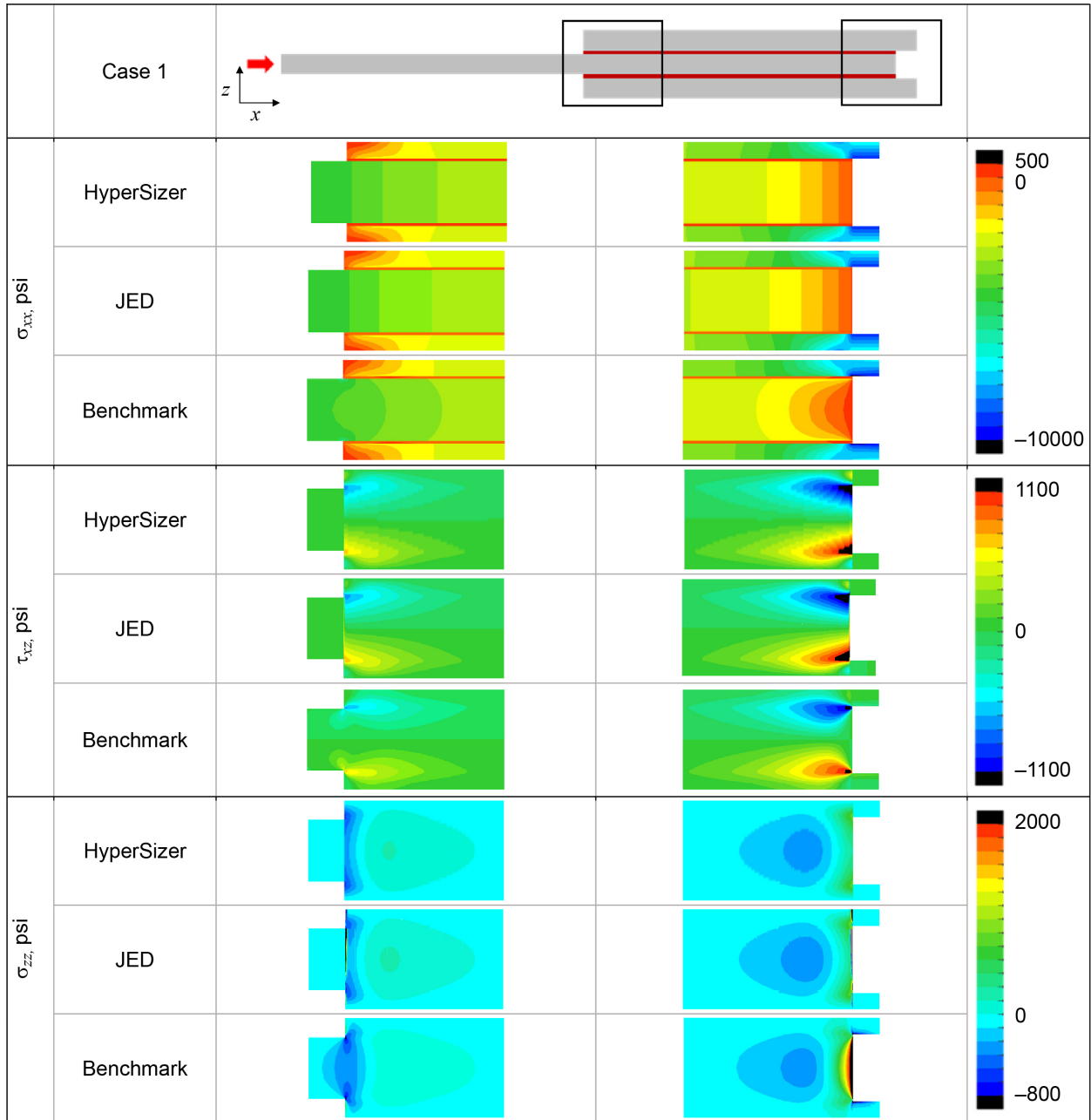


Figure 7.—Axial, out-of-plane, and shear stress contours for Case 1.

4.2 Case 2—Composite Adherends, No Steps, No Core

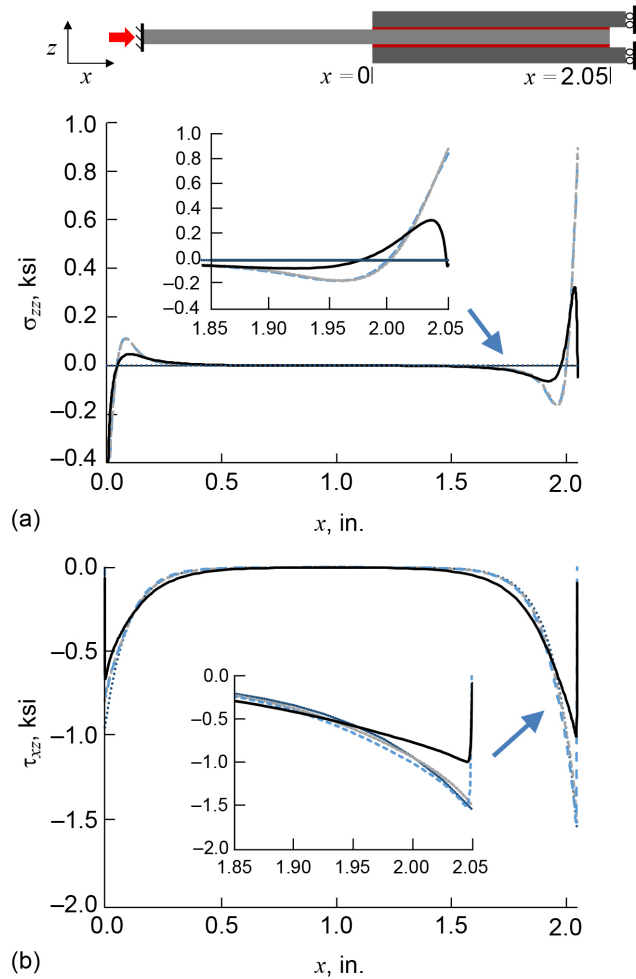


Figure 8.—Peel (a) and shear (b) stresses along the top adhesive centerline of Case 2.

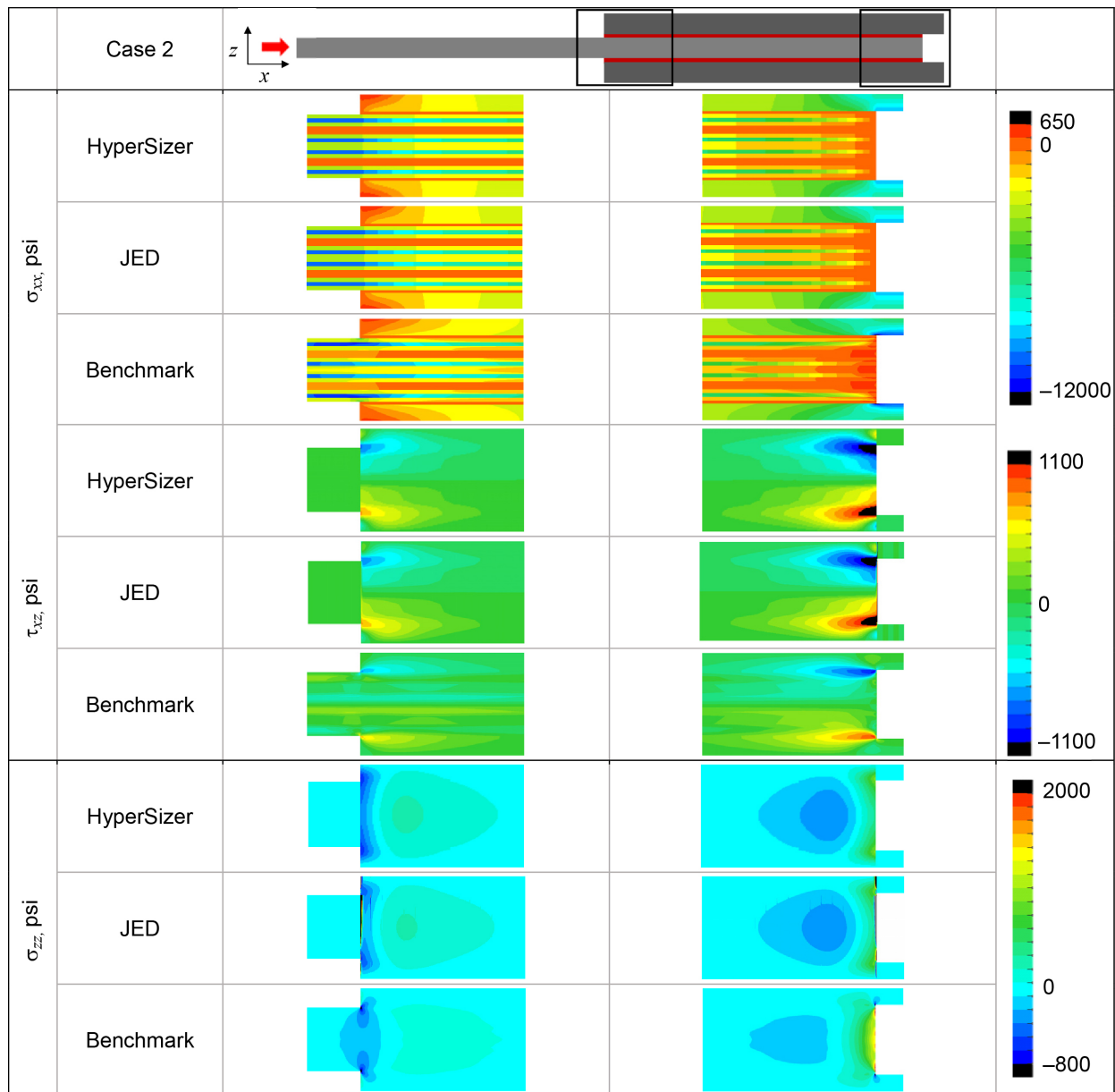


Figure 9.—Axial, out-of-plane, and shear stress contours for Case 2.

4.3 Case 3—Composite Adherends, Stepped Doublers, No Core

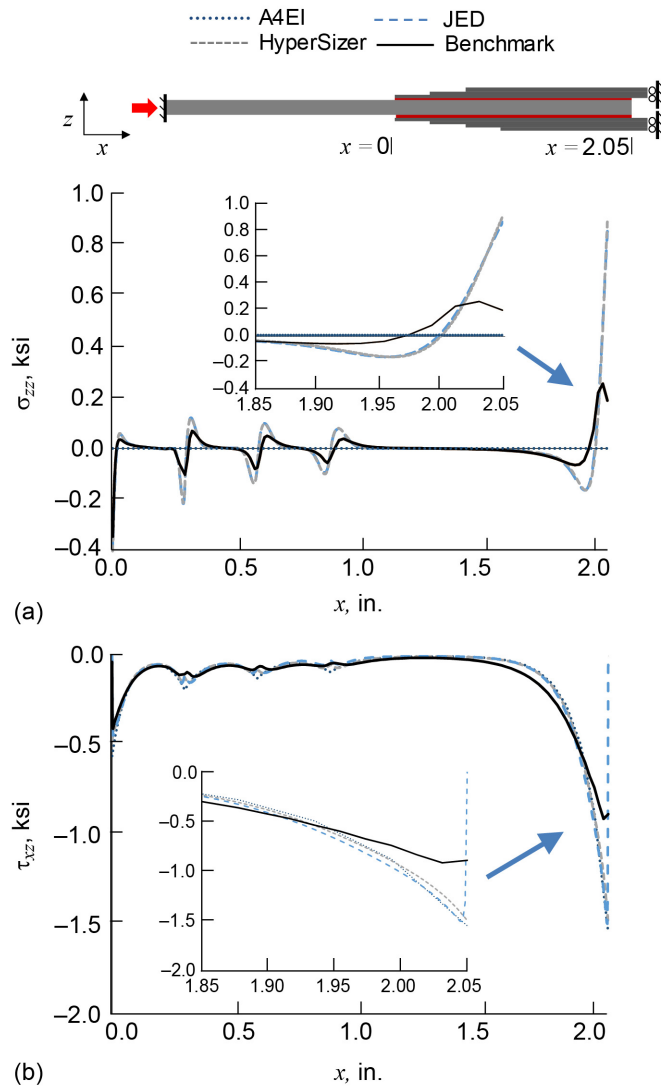


Figure 10.—Peel (a) and shear (b) stresses along the top adhesive centerline of Case 3.

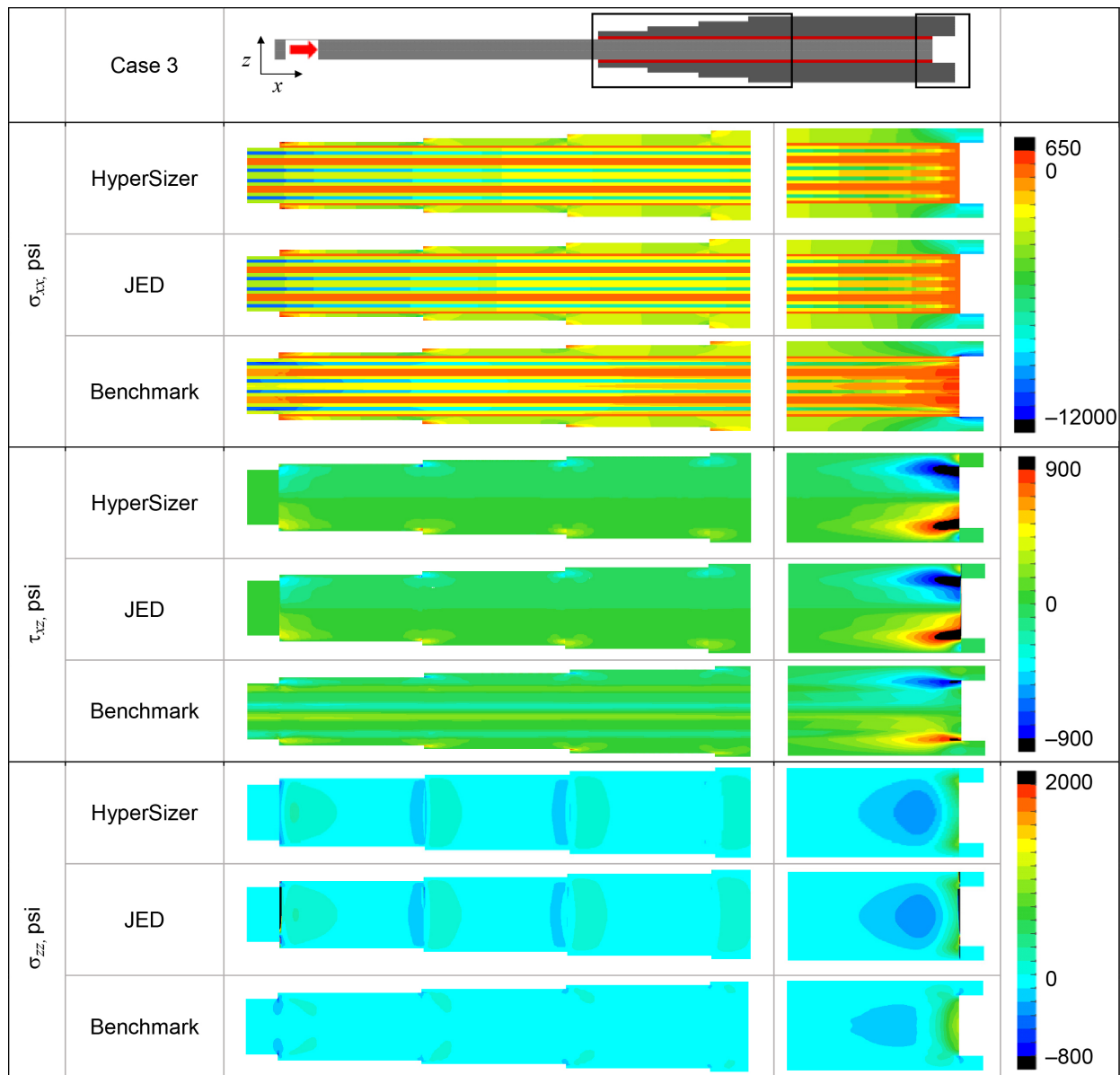


Figure 11.—Axial, out-of-plane, and shear stress contours for Case 3.

4.4 Case 4—Composite Adherends, No Steps, Honeycomb Core

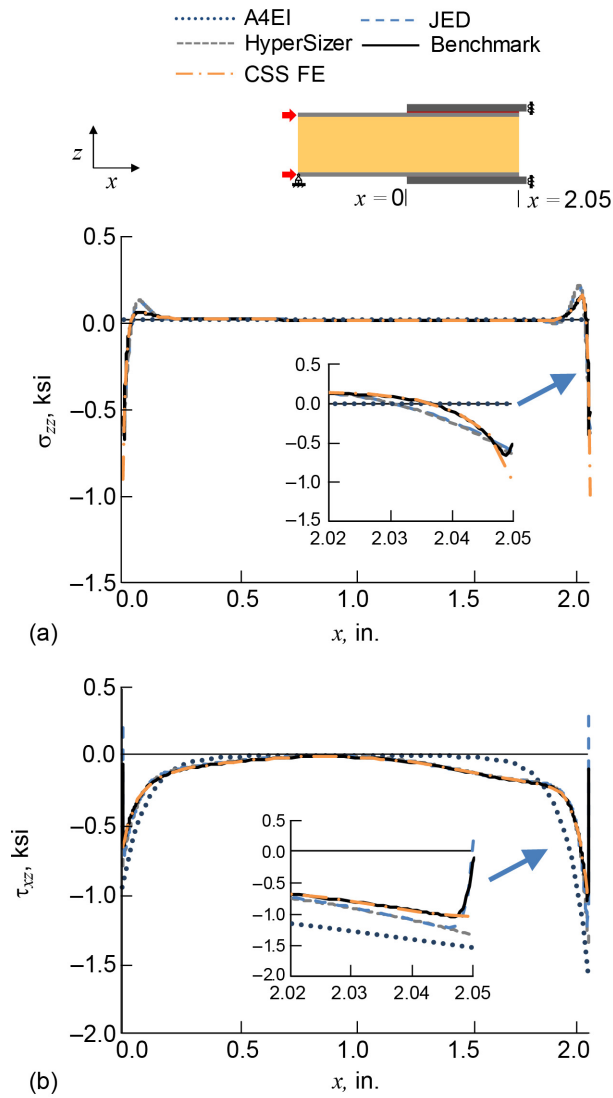


Figure 12.—Peel (a) and shear (b) stresses along the top adhesive centerline of Case 4.

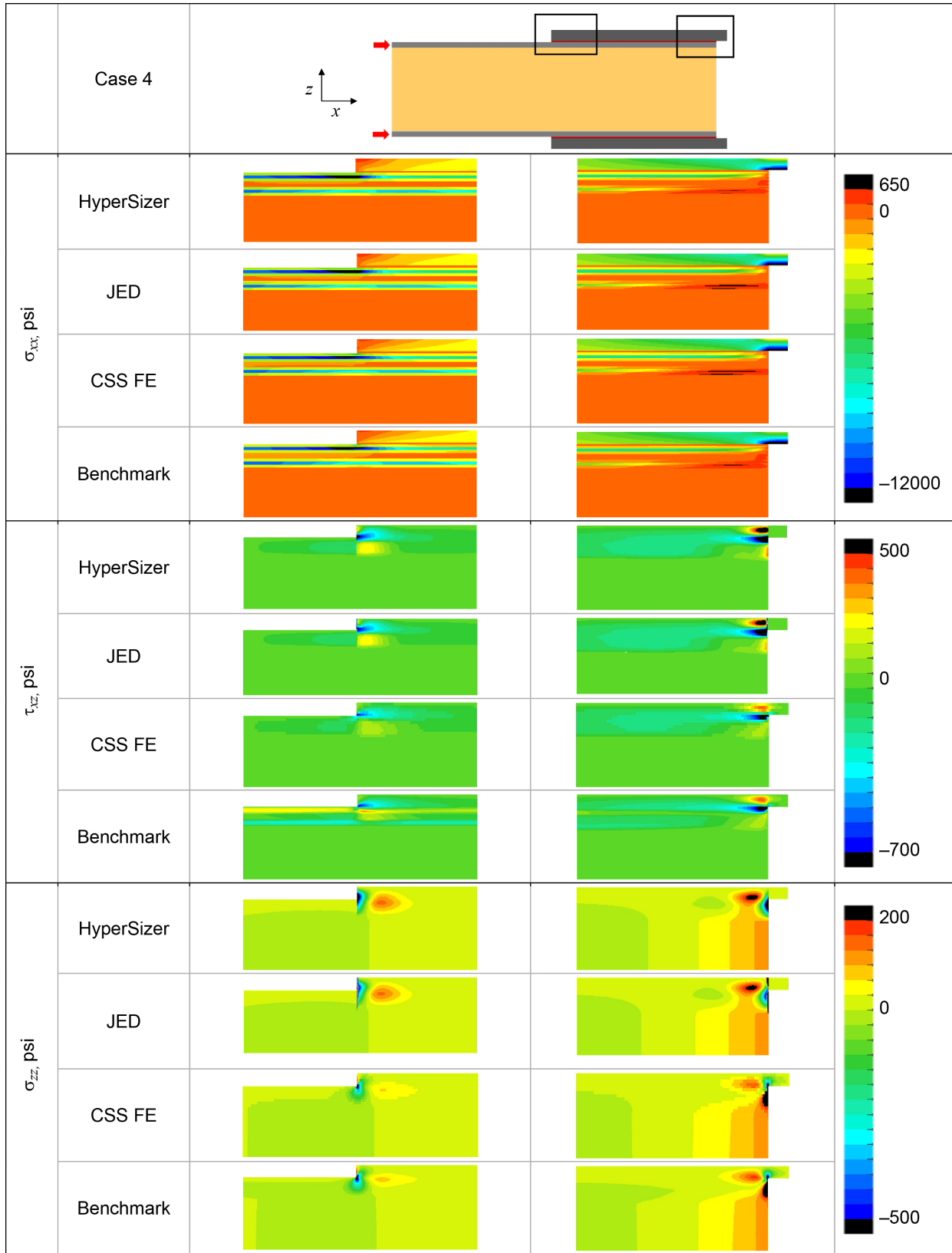


Figure 13.—Axial, out-of-plane, and shear stress contours for Case 4.

4.5 Case 5—Composite Adherends, Stepped Doublers, Honeycomb Core

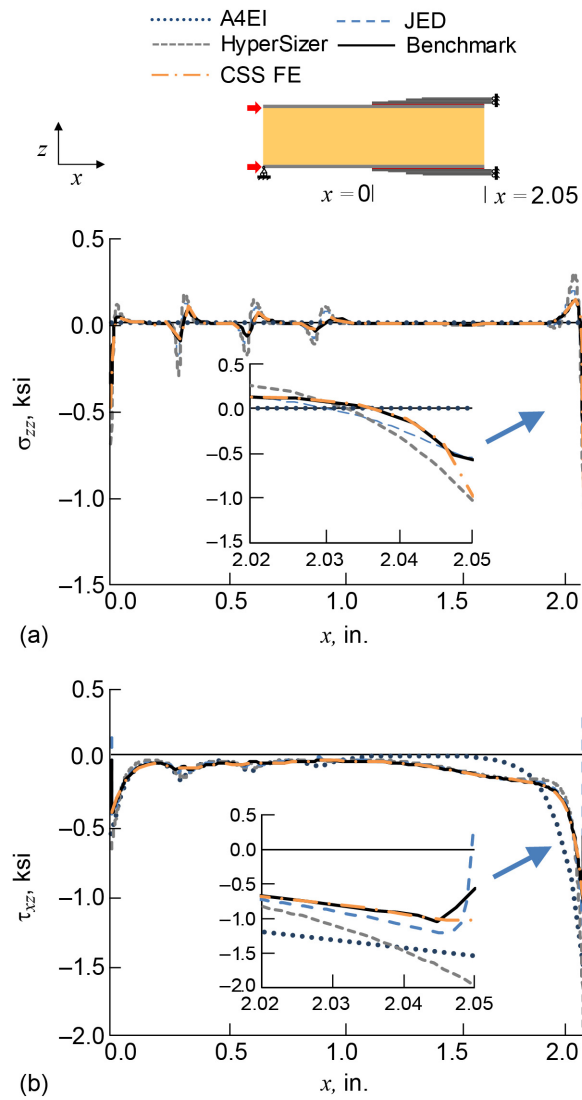


Figure 14.—Peel (a) and shear (b) stresses along the top adhesive centerline of Case 5.

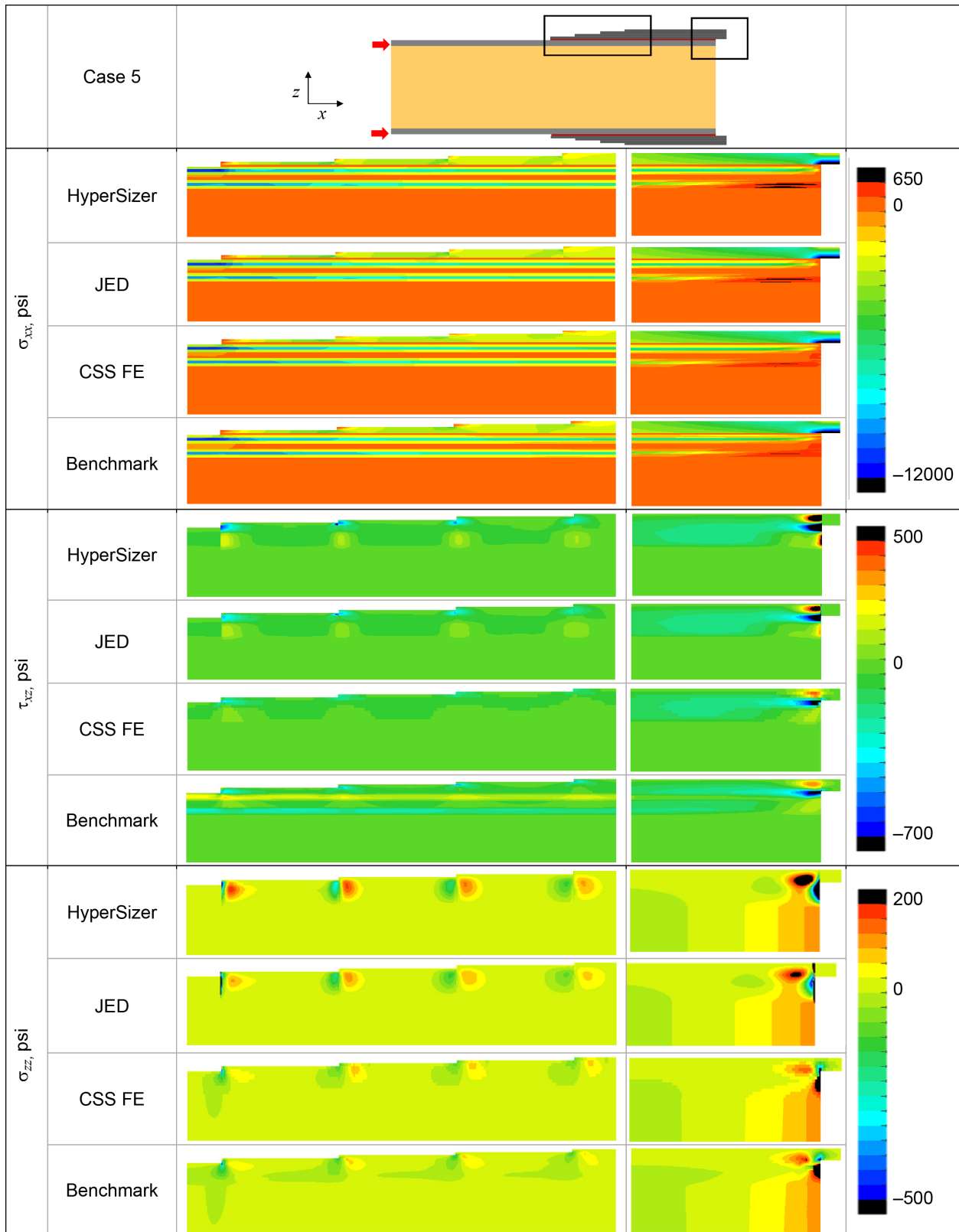


Figure 15.—Axial, out-of-plane, and shear stress contours for Case 5.

4.6 Case 6—Composite Adherends, Stepped Doublers, Honeycomb Core, Bending Loading

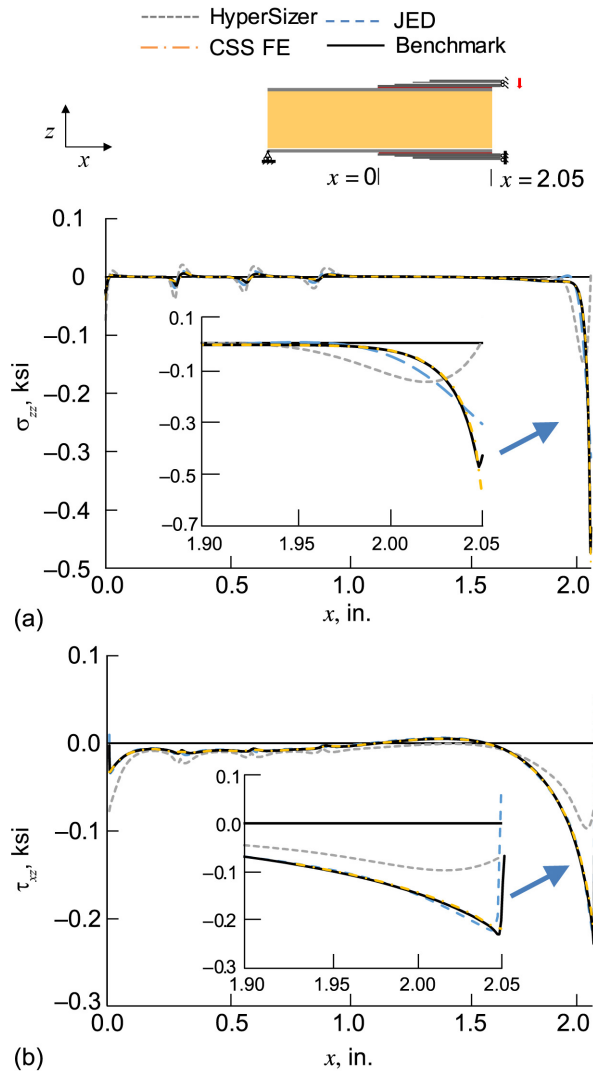


Figure 16.—Peel (a) and shear (b) stresses along the top adhesive centerline of Case 6.

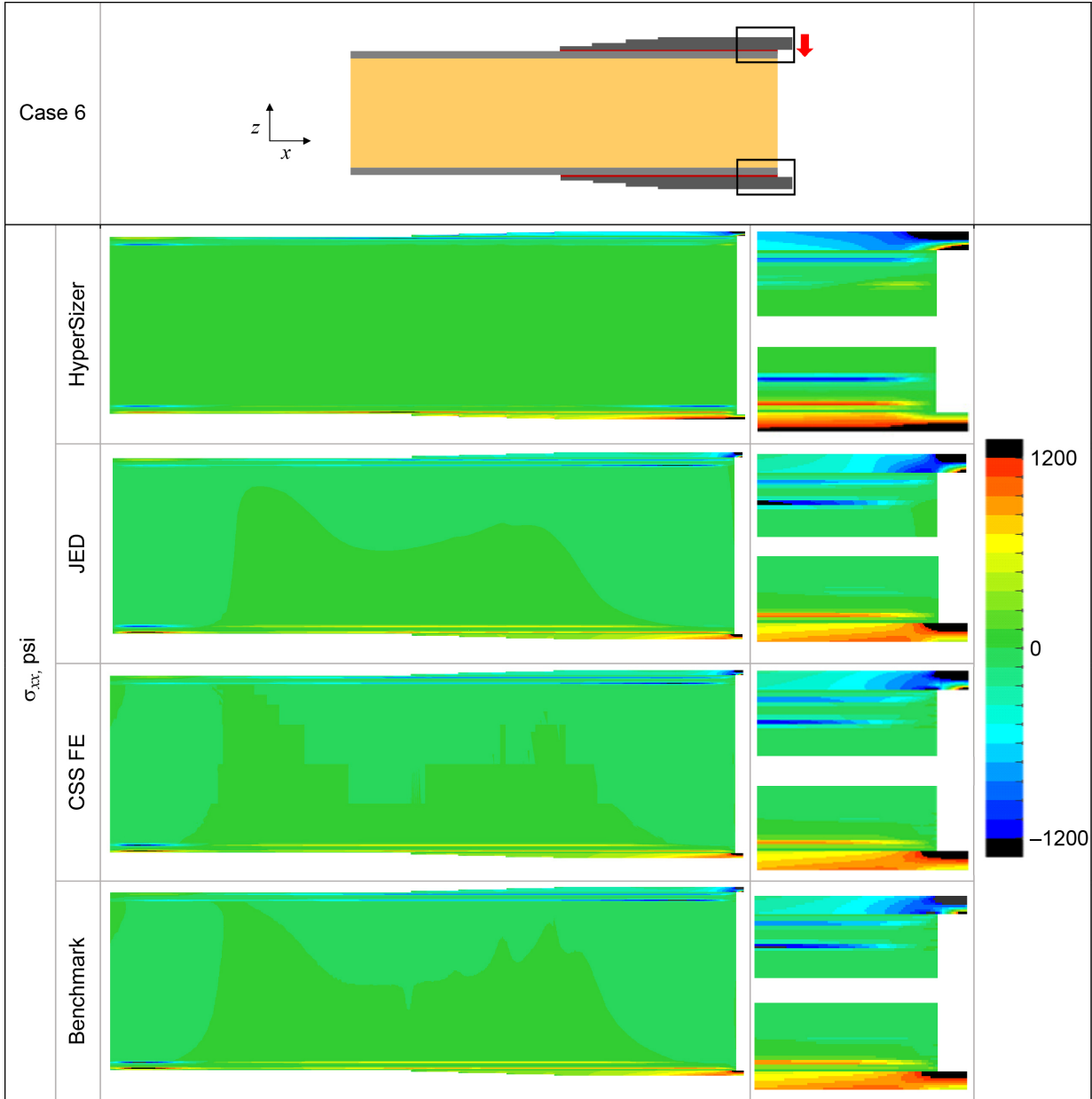


Figure 17.—Axial stress contours for Case 6.

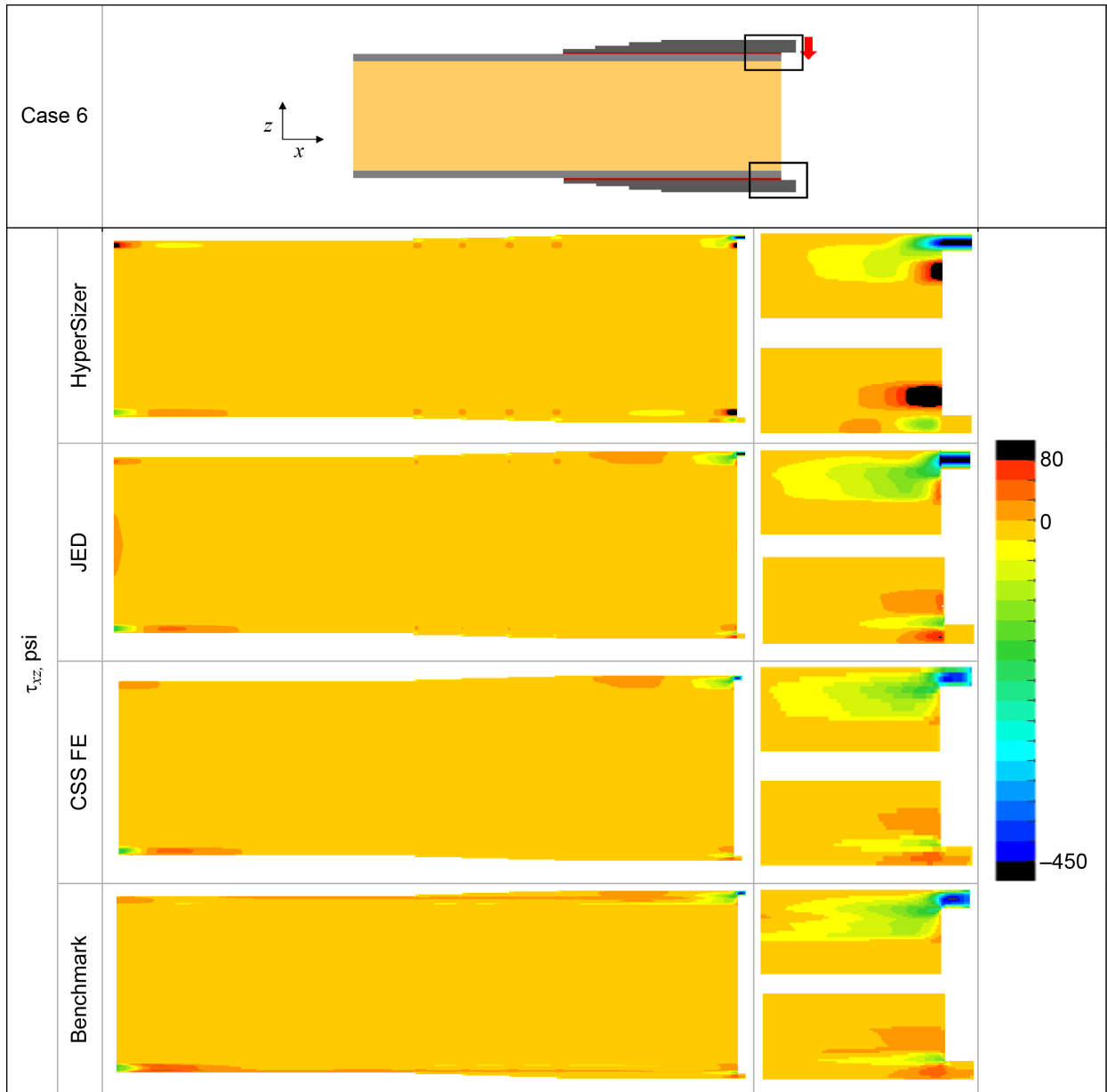


Figure 18.—Shear stress contours for Case 6.

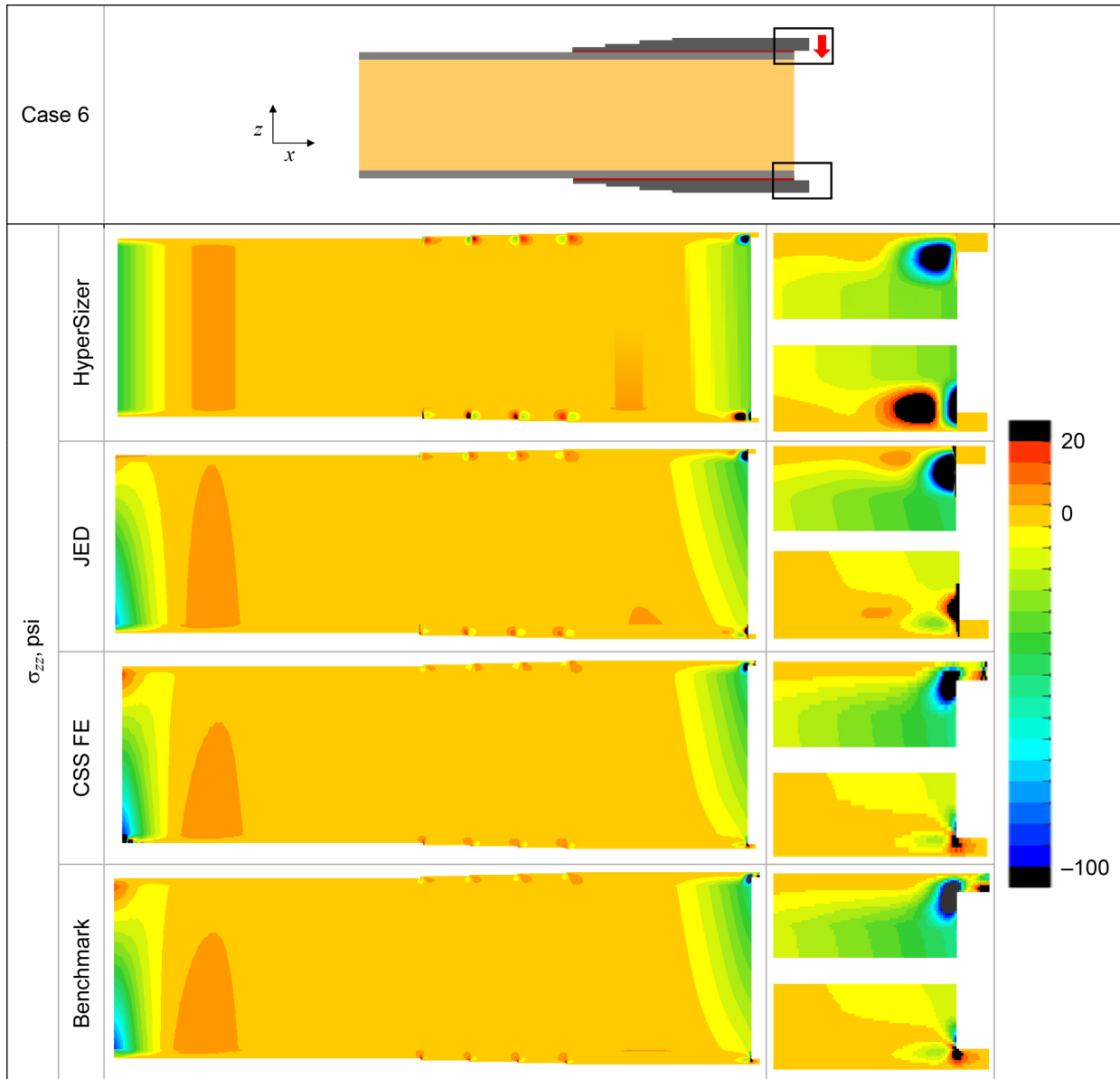


Figure 19.—Out-of-plane stress contours for Case 6.

5.0 Discussion

5.1 Comparison of Joint Configurations

One can compare the six considered cases with one another and observe what effect incremental changes in joint configuration can have on the stress distributions. First, looking at the difference between Cases 1 and 2 shows not only the difference between using composite and homogenous materials, but also materials with different stiffnesses. The bending stiffness (D_{11}) of Case 2 is 10 and 7 percent lower than Case 1 in the adherend and doubler, respectively. Similarly, the axial stiffness (A_{11}) is 5 and 7 percent lower in the adherend and doubler, respectively. As a result, the stress magnitudes for almost all stresses in Case 2 were generally lower in the adherend/doubler (Figure 7 and Figure 9). Even the peel and shear stresses in the adhesive were lower for Case 2 as shown in Figure 6 and Figure 8. This is particularly clear in the benchmark FEA peel stress results in the adhesive. The “trough” just before the

peel stress (σ_{zz}) begins to rise to the peaks are much lower in magnitude for Case 2. This is because the benchmark FEA model captures the effects of the 45° facesheet ply adjacent to the adhesive. The analytical models determine the adhesive stresses based on the homogenized adherend laminate properties and therefore do not capture these effects.

The effect of tapering the doubler can be seen by comparing Cases 2 and 3 and Cases 4 and 5. For the adhesive stresses, the taper decreases the peel and shear stress concentrations near the taper as would be expected. The stresses in the middle of the joint ($x = 2.05$ in.) do not appear to be heavily influenced by the taper, which for this particular joint is the critical region. In practice, inserts or gap fillers are applied in the gaps (open area between facesheets on right hand side of figures) to lower the stress concentration, but this gap area remains a critical region. For the adherend/doubler stresses, the taper lowers the peak shear near the taper but has little impact elsewhere. There is an even more drastic reduction in interlaminar peel stress (σ_{zz}) due to the taper. The peak axial stresses did not appear to be largely affected.

Similarly, comparing Cases 2 and 4 and Cases 3 and 5 can lead to general observations about the difference in stresses by adding a core. For adhesive stresses, the peel stress becomes slightly more concentrated in at the ends and even changes signs in the middle for the sandwich joints from tension to compression. The adhesive shear stress is more spread out for the sandwich joints, but the magnitude of the peak is not greatly impacted. For the adherend stresses, the sandwich cases generally had lower out-of-plane stresses. This is to be expected, because the core is relatively compliant in shear and transverse direction, which relieves much of the peel and shear stress built up in the adherend/doubler of the nonsandwich joints. The adherend/doubler axial stresses seem to be somewhat higher for the sandwich cases, but not drastically.

5.2 Discussion of A4EI

The A4EI results reflect the fact that this legacy tool is considerably more limited than the other analysis tools included in the study. A4EI does not predict adhesive peel stresses nor the stress fields in the adherends, and thus A4EI results can only be compared for the adhesive shear stress. In addition, the shear loading of Case 6 cannot be applied in A4EI, so no results are shown for the tool in that case. The adhesive shear stress predicted by A4EI is in reasonably good agreement with the benchmark FEA and the other tools. As with JED and HyperSizer, A4EI's noncontinuum spring representation of the adhesive does not allow it to predict the reversals in the shear and peel stress at the free edge that are predicted by the benchmark FEA. In the cases with the core, A4EI overpredicts the peak adhesive peel stress near the right edge. This tendency to be conservative might explain why the tool has been successfully employed for bonded joint design for many years despite not providing any of the details of the other tools considered herein.

5.3 Discussion of HyperSizer

For most of the cases examined, JED and HyperSizer produced very similar results, and both are in reasonably good agreement with the benchmark solution. This is due to similar underlying assumptions of beam-like behavior for the adherends and distributed springs to represent adhesives. The benchmark FEA, in contrast, is a full continuum solution, which illustrates some effects not captured by the more simplified models. Of particular interest is the behavior of the transverse shear stress τ_{xz} at the re-entrant corners of the cases studied. The benchmark solution clearly demonstrates that this τ_{xz} traction must equal zero at the free edge (of both adherends and adhesives), whereas neither HyperSizer nor JED enforce this behavior at free edges normal to the x -direction. The result is, at times, appreciably higher peak stresses at

the edges predicted by the simplified tools in both τ_{xz} and σ_{zz} , the latter of which being affected by the former.

In Case 1 (Figure 6 and Figure 7), the in-plane σ_{xx} appears to vary quadratically through the thickness of the center adherend in the benchmark case, while being represented as constant through the thickness for JED and HyperSizer. Both of the rapid tools use the classical lamination theory assumptions of linear in-plane stresses through the thickness of each ply within the adherends. In the case of a single “ply” with no bending (as in Case 1 center adherend), the result is a constant through-thickness σ_{xx} . For both Cases 1 and 2 (Figure 6 to Figure 9), the lower-order representation of σ_{xx} results in some differences in the details of the derived τ_{xz} and σ_{zz} fields when compared to the benchmark FEA. It is also of note that the over-prediction of the peak τ_{xz} and σ_{zz} in the adhesive (and related under-prediction of the “trough” prior to the peak in the adhesive σ_{zz}) is much greater in the Case 2, in which the adherends are composites rather than isotropic aluminum. This is because, as mentioned previously, the HyperSizer method cannot capture the effect of the compliant 45° facesheet ply adjacent to the adhesive.

For Case 3 (Figure 10 and Figure 11), although both JED and HyperSizer capture the effect of the moment introduced at ply drop locations, they overpredict the peak stresses and re-entrant corner τ_{xz} and σ_{zz} . This difference is again due to the benchmark FEA capturing the zero τ_{xz} at x -direction free-edges, whereas this cannot be achieved for the other tools. Still, both JED and HyperSizer do quite a good job of reproducing the benchmark FEA stress fields.

Cases 4 and 5 (Figure 12 to Figure 15) exhibit the same free-edge τ_{xz} effects noted for Case 3, but also demonstrate the impact of core compliance. The HyperSizer solution treats the core as an additional adhesive, resulting in zero core σ_{xx} and constant τ_{xz} through the core thickness. In contrast, the employed JED formulation results in quadratic τ_{xz} through the core thickness due to the quadratic displacement field. FEA, being a continuum solution with high density piecewise linear approximations of shape and displacements in either direction, may produce more complex distributions in both the core and the adherends. For example, for Case 4, HyperSizer matches the stresses in the adhesive quite well, but misses the reversal in τ_{xz} just adjacent to the free right edge (Figure 12). Examining the Case 4 stress fields in this vicinity (Figure 13), HyperSizer predicts a positive τ_{xz} peak in the top facesheet at the right free edge. In reality, τ_{xz} is a traction at this free edge and must be zero. The benchmark FEA captures this as, when approaching the right free edge in the top facesheet, the τ_{xz} first rises slightly and then rapidly approaches zero. In HyperSizer, the adherend σ_{zz} is calculated by integrating $d\tau_{xz}/dx$ (Ref. 14), therefore, directly at the right free edge of the top facesheet, HyperSizer predicts compressive σ_{zz} , whereas the benchmark FEA indicates that this stress is tensile. It should be noted, however, that, in practice, the joint geometry will not match the idealized geometry employed by any of the tools. Particularly at a free edge in the vicinity of the bondline, imperfections and features like the spew fillet will influence these very local stress features described above.

Case 6 (Figure 16 to Figure 19) was chosen to be quite challenging for the HyperSizer solution. The loading mimics three-point bending, but the aspect ratio of the joint is approximately 4:1, thus the simulation is actually closer to short beam shear. The HyperSizer formulation is based on plates in bending connected by continuous normal and shear springs. Furthermore, the load path is through the core (which is usually avoided in practice), further amplifying the impact of the core formulation. That being said, HyperSizer still does a decent job of reproducing the benchmark FEA stresses, particularly for the top of the joint in the vicinity of the load application. In concordance with the previous cases, HyperSizer still over predicts the peak stresses and predicts a peak τ_{xz} at the right free edge of the top facesheet. At the right bottom of the joint, the disparity between HyperSizer and the benchmark FEA is greater. Examining the σ_{xx} fields predicted by the benchmark FEA in this vicinity (Figure 17), it is

interesting that the z -direction distribution of σ_{xx} in the free hanging portion of the bottom adherend is opposite of what one would expect if the joint were dominated by bending. That is, the peak tensile σ_{xx} is at the top face rather than the bottom face in the Benchmark FEA. HyperSizer, on the other hand, predicts the trend that would be expected based on its bending formulation. This difference in σ_{xx} then results in further discrepancies in the τ_{xz} and σ_{zz} predicted by HyperSizer near the bottom right of the joint. However, examining the stress fields throughout the joint in Case 6, HyperSizer generally still does quite a good job of reproducing the benchmark FEA results.

5.4 Discussion of JED

The previous discussion on the HyperSizer model is mostly applicable for the JED model as well. One of the main differences is the quadratic distribution of the adhesive/core displacements in the z -direction. This difference means that the adhesive shear stress falls to near zero at the ends of the adhesive (see for example Figure 8), and the peel stress rises near the reentrant corner (top corner of the adhesive) and falls in the other direction (bottom corner of adhesive). Since the out-of-plane stresses are calculated based on integrating from the stress state of the neighboring adhesive, the extreme stress gradient at the corners results in large stresses in the doubler (see for example τ_{xz} and σ_{zz} for Case 4, Figure 13). These abnormally high stress concentrations in the doubler do not seem to reflect the mechanics of the problem nor reflect the benchmark model. This might have to do with the fact that using a second order model is not necessarily appropriate for a thin adhesive layers, and seems to start having a similar problem of a stress concentration as the continuum models. Though the current JED version requires the entire element to have the same model for the adhesive/core layers, it would be advisable in the future to have a linear interpolation for the adhesive while keeping a quadratic interpolation for the core.

5.5 Discussion of CSS FE

The CSS FE model performed very well as compared with the benchmark results for the three cases in which it was exercised (Cases 4 to 6). Generally good agreement with the benchmark FEA was expected since the two models are similar in many respects, with the main differences being the discretization and element types. For case 4, the adhesive stresses showed excellent quantitative agreement with the only discrepancies being located immediately at the reentered corners (Figure 12). Since CSS FE mesh included a single element through the thickness of the adhesive, it was unable to predict the stress reversals in τ_{xz} and σ_{zz} in the adhesive near the free edge. The contour plots show very good agreement with the benchmark results in general. Minor differences are noted in σ_{xx} and τ_{xz} in the composite facesheets as compared with the benchmark FEA. In cases where the CSS FE differs from the benchmark it appears to be in good agreement with HyperSizer and JED, likely due to the relatively coarse (as compared to the benchmark) approximation of the continuum solution afforded by using one CSS8 element per ply. Cases 5 and 6 exhibit similar features as Case 4 in terms of the comparison of the CSS FE with the benchmark. In some cases the stress is overpredicted (e.g., peak values of σ_{zz} near the reentered corner) whereas in other cases the stress is underpredicted (e.g., τ_{xz} and σ_{zz} at ply terminations). Although the model generally predicts the stress fields accurately, the locations where differences between the CSS FE results and the benchmark results occur are the hotspot locations where local minimum margins would be calculated for the purpose of design. Therefore, careful selection and interpretation of the stress fields and peaks is required.

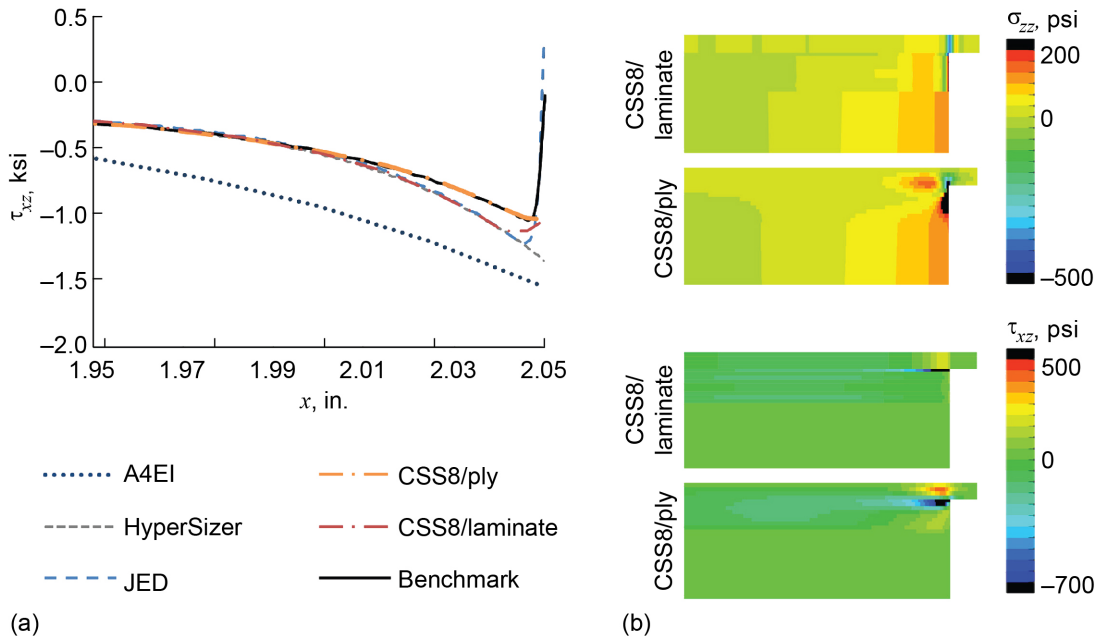


Figure 20.—Effect of through the thickness mesh refinement on the CSS FE model stress fields for Case 4.

A simplification of the CSS FE model where the composite facesheets and doublers were each modeled with one layer of continuum solid shell elements through the thickness was also explored for Case 4. The plies in the facesheet and doubler were represented using a composite section definition with three integration points per ply. Comparison of the results from the two versions of the model highlights the effect of treating the laminates like beams (as is done by HyperSizer and JED) versus continuum on the adhesive stresses as show in Figure 20(a). The shear stress predicted in the adhesive agrees with HyperSizer and JED predictions when one element through the thickness of the laminates is used. When one element per ply is used, the shear stress in the adhesive matches the benchmark result. The same trends were found for the peel stress and for the other cases. The stress fields in the adherends show a starker contrast between the two versions of the CSS FE model. Since the continuum solid shell elements assume a constant peel and shear strain through the thickness, simplifying the model to one element through the thickness of the laminate yields in a significant loss of fidelity in the adherend stress shear and peel fields as shown in Figure 20(b). Therefore, in most cases, simplifying to one continuum solid shell element per laminate appears invalid.

5.6 Comparing Peak Adhesive Stresses

One aspect worthy of discussion is the comparison of adhesive stresses near the stress concentrations. The continuum-based FE models have stresses that vary through the thickness of the adhesive and stress singularities at the reentrant corner, which can never be resolved with a refined mesh. Meanwhile, spring-based models like the HyperSizer and JED models do not have the problem of stress singularities since the adhesive is given an interpolation function through the thickness (linear for HyperSizer, quadratic for JED) and do not enforce stress-free boundary conditions at the ends of the adhesive. To compare these two types of models is problematic at best, and tradition has dictated that stresses at the centerline of the continuum models are used for the comparison. However, continuum-based FE models show that there is a strong stress gradient through the thickness at the ends of the adhesive, which makes the comparison

somewhat arbitrary. The root of the problem lies in the fact that the most critical point of the adhesive is the point at which a strong comparison cannot be made.

To overcome this limitation and to dispel some of the ambiguity of stresses in this region, many have used the concept of a “characteristic distance”. In this approach, the stresses are compared at a characteristic distance from the edge, with one of many definitions of this distance being the thickness of a ply. For the cases shown here, the distance would be around 0.007 in., and some cases look like the stresses are independent of edge effects at the distance (for example Figure 12) but for others, the stress predictions have already diverged due to the boundary (Figure 10). This may be a good example of why using the characteristic distance for comparing continuum-based FE models with spring-based models may be problematic.

Furthermore, the characteristic distance has been used to predict strength for spring-type design models such as the HyperSizer or JED models. In this approach, a joint is tested experimentally, and, based on the failure load and a pre-determined characteristic distance, some form of a strength measurement is found. This is then used for other joints of the same material, with the strength considered to be a material property. One of the lessons of this study should be that such methods should be considered with caution.

6.0 Conclusions

This study compared four bonded joint design tools with a benchmark high fidelity FEA model for six different joint configurations. Three of the design models were ordinary differential equation based models (A4EI, HyperSizer, and JED), where beam theory and springs were used for the through-thickness interpolation of displacements, and the structural response was found by solving equilibrium in the axial direction. The fourth model (CSS FE) was an automated coarse-mesh FE model with continuum elements for the adhesive/core and solid shell elements for the adherends. The six different joint configurations were derived from one joint configuration with a bonded sandwich panel under axial compression loading (Case 5), with Case 6 being the same configuration under bending, and the other four configurations derived by removing either the doubler stepped ply drop (Cases 4 and 2), sandwich core (Cases 3 and 2), or layered composite adherends (Case 1).

The capabilities of A4EI are considerably fewer than the other tools, and it is able only to predict the adhesive shear stress for inclusion in the comparisons. These comparisons showed that A4EI’s adhesive shear stress prediction was reasonable, but not in as good agreement with the benchmark solution as the other design tools. Generally speaking, all of the other models were able to represent the stresses in the adhesive and adherend/doubler fairly consistently and accurately. When discrepancies arose, they were typically found in the regions of the reentrant corners, which are always problematic and, unfortunately, the most critical. The fact that the JED and HyperSizer models do not enforce traction-free boundaries for the core/adhesive meant higher stresses at the ends of the adhesive than the benchmark. Similarly, the CSS FE model only represented the adhesive with one element, which could not resolve the traction-free boundary either and matched up closely with the other models.

For the adherend stress predictions, discrepancies with the benchmark were due to the assumption of displacement variation through the thickness. HyperSizer and JED assume linear axial displacements through the thickness, and the CSS FE model assumes the same when one element through the adherend thickness is used. The error arising from this limitation were demonstrated by running the CSS FE model for one integrated layered element over the adherend thickness versus one element per ply. The model with one element per ply showed much better agreement with the benchmark.

Although adherend through-thickness stresses are assumed to be negligible for beam theory, an equilibrium-based approach for finding these stresses has been implemented in HyperSizer and JED with the results presented throughout the paper. The out of plane stress, σ_{zz} , is based on through-thickness integration of the x-derivative of the shear stress, τ_{xz} , making it sometimes sensitive to grid spacing.

The interpolation of displacements within the core and adhesive layers was another source of error. The HyperSizer model used linear interpolation, while the JED model used a quadratic interpolation. For Cases 1 to 5 this did not appear to have much of a difference other than the fact that the shear stresses for the JED model went near 0 at the ends of the adhesive. However, when shear in the core was the dominant mode as in Case 6, the core was not sufficiently represented with linear displacements and larger discrepancies with the benchmark resulted.

Although there are discrepancies between the design models and the benchmark, it is important to keep two things in mind. (1) It is very unlikely that joints in practice have completely sharp reentrant corners and ply drops, which lead to a stress singularity in models, so spending effort to resolve this difference may not be worthwhile. (2) These models are design models, so they are built for speed rather than purely for accuracy. The design models all had runtimes in the order of seconds to minutes, orders of magnitudes faster than the benchmark. Therefore, when evaluating runtime, one must also consider pre and post processing time, which can dwarf processing time. All of the design models featured here have been automated in some form with easy and clear methods for extracting results. Therefore, as long as limitations highlighted here are kept under consideration, these design models can enable parametric studies, sizing studies, and joint configuration comparisons for adhesively bonded joints.

References

1. Bell, S., "Structural adhesives deliver lighter composite structures with performance and costs benefits," Reinforced Plastics, Feb. 2012.
2. Hart-Smith, L.J., "Adhesive-bonded single-lap joints," NASACR112236, 1973, p. 116.
3. Hart-Smith, L.J., Adhesive-bonded double-lap joints. [analytical solutions for static load carrying capacity], 1973.
4. Mortensen, F., and Thomsen, O.T., "Analysis of adhesive bonded joints: a unified approach," Composites Science and Technology, vol. 62, Jun. 2002, pp. 1011–1031.
5. Stapleton, S.E., and Waas, A.M., The Analysis of Adhesively Bonded Advanced Composite Joints Using Joint Finite Elements, Cleveland, OH: NASA Glenn Research Center, 2012.
6. Wanthal, S., "Verification and Validation Process for Progressive Damage and Failure Analysis Methods in the NASA Advanced Composites Consortium," West Lafayette, IN, United States: 2017.
7. Man, M., Cytec Cycom 5320-1 T650 3k-PW Fabric Qualification Material Property Data Report, Wichita, KS: National Institute for Aviation Research, 2015.
8. "PAMG-XR1 5056 Aluminum Honeycomb," Rev. 6.19.18, 2018.
9. Leone, F.A., Dávila, C.G., and Girolamo, D., "Progressive damage analysis as a design tool for composite bonded joints," Composites Part B: Engineering, vol. 77, Aug. 2015, pp. 474–483.
10. Hart-Smith, L.J., Company, D.A., and Center, L.R., Analysis and design of advanced composite bonded joints, National Aeronautics and Space Administration, 1974.
11. HyperSizer, Collier Research Corp., <https://hypersizer.com/>, 2018.
12. Yarrington, P., Zhang, J., Collier, C., and Bednarczyk, B., "Failure Analysis of Adhesively Bonded Composite Joints," Austin, Texas: American Institute of Aeronautics and Astronautics, 2005.

13. Yarrington, P., Collier, C., and Bednarczyk, B., "Failure Analysis of Adhesively Bonded Composite Joints via the Virtual Crack Closure Technique," 47th AIAA/ASME/ASCE/AHS/ASC Structures, Structural Dynamics, and Materials Conference, American Institute of Aeronautics and Astronautics.
14. Bednarczyk, B., Bansal, Y., Collier, C., Pindera, M.-J., and Zhang, J., "Analysis Tools for Adhesively Bonded Composite Joints, Part 1: Higher-Order Theory," *AIAA Journal*, vol. 44, 2006, pp. 171–180.
15. Zhang, J., Bednarczyk, B.A., Collier, C.S., Yarrington, P.W., Bansal, Y., and Pindera, M.-J., "Analysis Tools for Adhesively Bonded Composite Joints, Part 2: Unified Analytical Theory," *AIAA Journal*, vol. 44, Aug. 2006, pp. 1709–1719.
16. Stapleton, S.E., Waas, A.M., and Bednarczyk, B.A., "Bonded Joint Elements for Structural Modeling and Failure Prediction," 52nd AIAA/ASME/ASCE/AHS/ASC SDM Conference, Denver, CO: 2011.
17. Frostig, Y., Baruch, M., Vilnay, O., and Sheinman, I., "High-Order Theory for Sandwich-Beam Behavior with Transversely Flexible Core," *Journal of Engineering Mechanics*, vol. 118, 1992, pp. 1026–1043.
18. Stapleton, S.E., Waas, A.M., Arnold, S.M., and Bednarczyk, B.A., "Corotational Formulation for Bonded Joint Finite Elements," *AIAA Journal*, vol. 52, 2014, pp. 1280–1293.
19. Stapleton, S.E., Weimer, J., and Spengler, J., "Design of functionally graded joints using a polyurethane-based adhesive with varying amounts of acrylate," *International Journal of Adhesion and Adhesives*, vol. 76, Jul. 2017, pp. 38–46.
20. Stapleton, S.E., Waas, A.M., and Arnold, S.M., "Functionally graded adhesives for composite joints," *International Journal of Adhesion and Adhesives*, vol. 35, Jun. 2012, pp. 36–49.
21. Moler, C., and Van Loan, C., "Nineteen Dubious Ways to Compute the Exponential of a Matrix, Twenty-Five Years Later," *SIAM Review*, vol. 45, 2003, p. 3.
22. Vu-Quoc, L., and Tan, X.G., "Optimal solid shells for non-linear analyses of multilayer composites. I. Statics," *Computer Methods in Applied Mechanics and Engineering*, vol. 192, Feb. 2003, pp. 975–1016.
23. Smith, M., *ABAQUS/Standard User's Manual*, Version 2017, Providence, RI: Simulia, 2016.

